The Journal of Immunology

Anatomical Location Determines the Distribution and Function of Dendritic Cells and Other APCs in the Respiratory Tract

Christophe von Garnier, Luis Filgueira, Matthew Wikstrom, Miranda Smith, Jennifer A. Thomas, Deborah H. Strickland, Patrick G. Holt and Philip A. Stumbles

J Immunol 2005; 175:1609-1618; ;
doi: 10.4049/jimmunol.175.3.1609
http://www.jimmunol.org/content/175/3/1609

The Journal of Immunology is published twice each month by
The American Association of Immunologists, Inc.,
1451 Rockville Pike, Suite 650, Rockville, MD 20852

Print ISSN: 0022-1767 Online ISSN: 1550-6606.

Anatomical Location Determines the Distribution and Function of Dendritic Cells and Other APCs in the Respiratory Tract[1]

Christophe von Garnier,[2]* Luis Filgueira,[†] Matthew Wikstrom,* Miranda Smith,* Jennifer A. Thomas,* Deborah H. Strickland,* Patrick G. Holt,* and Philip A. Stumbles[2,3]*

APCs, including dendritic cells (DC), are central to Ag surveillance in the respiratory tract (RT). Research in this area is dominated by mouse studies on purportedly representative RT-APC populations derived from whole-lung digests, comprising mainly parenchymal tissue. Our recent rat studies identified major functional differences between DC populations from airway mucosal vs parenchymal tissue, thus seriously questioning the validity of this approach. We addressed this issue for the first time in the mouse by separately characterizing RT-APC populations from these two different RT compartments. CD11c^{high} myeloid DC (mDC) and B cells were common to both locations, whereas a short-lived CD11c^{neg} mDC was unique to airway mucosa and long-lived CD11c^{high} macrophage and rapid-turnover multipotential precursor populations were predominantly confined to the lung parenchyma. Airway mucosal mDC were more endocytic and presented peptide to naive CD4$^+$ T cells more efficiently than their lung counterparts. However, mDC from neither site could present whole protein without further maturation in vitro, or following trafficking to lymph nodes in vivo, indicating a novel mechanism whereby RT-DC function is regulated at the level of protein processing but not peptide loading for naive T cell activation. ***The Journal of Immunology,*** **2005, 175: 1609–1618.**

The respiratory tract (RT)[4] is continuously exposed to a vast array of environmental Ags, ranging from harmless protein to potentially harmful pathogens. Discrimination between proteins and pathogens at this site therefore represents a continual challenge to the local airway mucosal immune system. In healthy individuals, nonreactivity or active tolerance to inhaled innocuous non-self-Ags normally arises as a default response to repeated exposure (1, 2). However, this immunological equilibrium can be disrupted following infection or in atopic disorders, such as allergic asthma, generating an inappropriate and potentially tissue-damaging responses to intrinsically nonpathogenic allergens (3, 4).

Control of the balance between tolerance and immunity in the RT is believed to be a process primarily directed by RT-dendritic cells (RT-DC) (5). RT-DC have been identified in both the airway mucosa and lung parenchyma of rodents and humans where they are thought to play distinct roles in control of immunological homeostasis to inhaled Ags (5, 6). In the airway mucosa, RT-DC form a tight network throughout the epithelium and underlying lamina propria, being ideally situated to sample inhaled Ags. In addition, much larger populations of RT-DC are also present in the lung parenchyma and alveolar spaces of the lower RT. In addition to RT-DC, a variety of APC types are also present in the RT, including B cells (7) and macrophages (mϕ), which in some circumstances can express high levels of immunosuppressive activity (8). Within the lung parenchyma, RT-DC are in close contact with alveolar and parenchymal tissue mϕ. Although mϕ are not thought to typically play a role in Ag traffic to lymph nodes, they are capable of suppressing DC function, thereby preventing local T cell activation and ensuing inflammation (8–10).

A significant degree of DC heterogeneity has been described in mice, with at least five distinct subpopulations identified in lymph nodes and spleen based on coexpression of CD11c with other surface markers such as MHC class II, CD4, CD8α, CD11b, and CD205 (11). These include three subsets of myeloid DC (mDC) distinguished by differential expression of CD4, CD11b, CD205, and CD8α^+ DC that express homodimers of CD8α together with high levels of CD205. Additional subsets include plasmacytoid DC (pDC; B220$^+$, Gr-1$^+$, 120G8$^+$) in all lymph nodes (12, 13) and epidermal Langerhans cells (CD8$^-$CD205$^+$) in those draining the skin (14). In contrast, despite their abundance in local tissues, very limited information is available regarding the types of DC subsets present in the RT. Furthermore, their relative distribution within differing anatomical compartments of the mouse RT, and the presence of other APC within these sites, has received little attention. For largely technical reasons, mouse studies to date have focused almost exclusively on more readily available populations obtained in total lung digests.

In this study, we have used a combination of multiparameter surface phenotyping, transmission electron microscopy (TEM), and functional characterizations to delineate RT-APC populations and determine their distribution within the main anatomical compartments of the murine RT. Using this approach, we describe a previously unrecognized complexity of RT-APC subpopulations present in the RT and demonstrate a distinct compartmentalization

*Telethon Institute for Child Health Research, Centre for Child Health Research and the School of Paediatrics and Child Health, University of Western Australia, Perth, and [†]School of Anatomy and Human Biology, University of Western Australia, Crawley, Western Australia, Australia

Received for publication January 7, 2005. Accepted for publication May 17, 2005.

The costs of publication of this article were defrayed in part by the payment of page charges. This article must therefore be hereby marked *advertisement* in accordance with 18 U.S.C. Section 1734 solely to indicate this fact.

[1] This work was supported by the National Health and Medical Research Council of Australia. C.v.G. was funded by the Swiss National Fund, Janggen-Poehn-Stiftung, Herrmann-Stiftung, Novartis-Stiftung, and Boehringer Ingelheim.

[2] Address correspondence and reprint requests to Dr. Christophe von Garnier or Dr. Philip A. Stumbles, Division of Cell Biology, Telethon Institute for Child Health Research, P.O. Box 855, West Perth, WA 6872, Australia. E-mail address: phils@ichr.uwa.edu.au or christophe@ichr.uwa.edu.au

[3] Current address: Division of Health Sciences, Murdoch University, Perth, WA 6150, Australia.

[4] Abbreviations used in this paper: RT, respiratory tract; DC, dendritic cell; pDC, plasmacytoid DC; mDC, myeloid DC; mϕ, macrophage; BALF, bronchoalveolar lavage fluid; TEM, transmission electron microscopy; DX, dextran; i.n., intranasal; DLN, draining lymph node; TBLN, tracheobronchial lymph node; PMLN, posterior mediastinal lymph node; ILN, inguinal lymph node; int, intermediate.

0022-1767/05/$02.00

between the differing anatomical locations. We also show that the definition of RT-DC in these locations must be made using a multiparameter approach and cannot rely solely on the expression of single markers such as CD11c. Contrasting with previous findings in the rat (15), steady-state mouse RT-DC demonstrated a high basal capacity for loading of free peptide onto MHC class II molecules for stimulation of naive $CD4^+$ T cells. Rather, the capacity to process intact protein Ag for presentation to naive T cells represented the key control point for regulation of the APC functions of mouse RT-DC. Finally, our mouse data support the conclusions from studies in other species that interactions between APC populations within the RT are important for the regulation of local immune reactivity to inhaled Ags.

Materials and Methods

Animals

BALB/c mice were bred specific pathogen free at the Animal Resource Centre (Perth, Australia) and housed under clean conditions at the Telethon Institute for Child Health Research (TICHR). BALB/c DO11.10 TCR transgenic mice recognizing an $I\text{-}A^d$-restricted epitope of OVA (peptide sequence ISQAVHAAHAEINEAGR) were purchased from The Jackson Laboratory and bred under clean conditions at the TICHR. All mice were used as females of 8–10 wk of age and given free access to feed and water. Animal experimentation was approved by the TICHR Animal Experimentation Ethics Committee, operating under guidelines set by the National Health and Medical Research Council of Australia.

Cell preparations from lung and conducting airways

Animals were euthanized by i.p. injection of 100 μl of phenobarbitone sodium (Lethabarb; Virbac). Lung and heart were exposed by bilateral thoracotomy, and the aorta and inferior vena cava were cut to exsanguinate animals before perfusion of the right ventricle with at least 5 ml of PBS. Thereafter, the peripheral third of the lung was excised (further referred to as lung parenchyma), and airways, including the trachea and the main bronchi (further referred to as main conducting airways), were prepared. Lung parenchyma was chopped into 2-mm slices using a McIlwain tissue chopper (Mickle Laboratory Engineering), and main conducting airways were manually sliced into thin pieces. Cell isolation procedures were conducted in a solution of 11 mM D-glucose, 5.5 mM KCl, 137 mM NaCl, 25 mM Na_2HPO_4, and 5.5 mM $NaH_2PO_4{\cdot}2H_2O$ (GKN) supplemented with 10% FCS as indicated. Tissue was transferred into 30 ml of GKN-10% FCS containing 1.8 mg/ml collagenase type 4 (Worthington Biochemical) and 0.1 mg/ml DNase I (Sigma-Aldrich) and incubated for 90 min at 37°C in a shaking water bath. After 60 min, an additional 0.1 mg/ml DNase I was added to the tracheal digests. Tissue was disrupted with a plastic transfer pipette until most of the larger tissue pieces were dispersed. The digest mixture was then passed through a cotton wool filter to remove tissue debris. After one wash in GKN-10% FCS, RBC lysis was performed with NH_4Cl and cells were resuspended in fluorescence buffer (PBS containing 0.5% BSA and 0.1% sodium azide) after one wash.

Staining for flow cytometry

Unless indicated otherwise, Abs were obtained from BD Pharmingen. Staining was performed on ice throughout the procedure. Cells were incubated with anti-Fc block (anti-mouse CD16/CD32) to reduce nonspecific binding 10 min before addition of the following anti-mouse Abs: PE-conjugated anti-CD11c and -CD69, FITC-conjugated anti-I-A/I-E (I-A/E), allophycocyanin-conjugated anti-CD11b, cytochrome-conjugated anti-CD4, biotinylated anti-CD2, -CD3ϵ, -CD4, -CD8α, -CD19, -CD40, -CD45RB, -CD80, -CD86, -CD205 (Cedarlane Laboratories), F4/80 Ag (Serotec), KJ1-26 (Caltag Laboratories), B220, Ly6G, and Ly6C (Gr-1). The rat IgG1 120G8 mAb recognizing mouse pDC (13) was kindly provided by Drs. G. Trinchieri and C. Asselin-Paturel (Schering Plough, Dardilly, France). Relevant isotype control Abs were used throughout. Streptavidin-conjugated fluorochromes, allophycocyanin, cytochrome, PerCP, FITC, PE, and PerCP cyanin 5.5 were purchased from BD Pharmingen. Cell samples were analyzed for surface fluorescence by flow cytometry using a FACSCalibur (BD Biosciences). Staining for surface molecules was reported as the frequency of cells within a population expressing the marker of interest, rather than mean fluorescence intensity levels due to variable autofluorescence (and therefore background staining) levels in different cell populations. For quantitative analysis of APC endocytotic activity, cells were resuspended in GKN-10% FCS containing 0.5 mg/ml FITC-conjugated dextran (DX-FITC; M_r = 40 kDa; Molecular Probes) for 90 min at 37 and 4°C. The reaction was interrupted by washes with ice-cold fluorescence buffer and endocytosis was determined by measuring FL1 fluorescence intensity in different APC populations. For the collection of bronchoalveolar lavage fluid (BALF), a small-bore catheter was inserted through a tracheostomy, and lungs were lavaged three times by slowly infusing and withdrawing a 1-ml volume of ice-cold PBS containing 2 mg/ml BSA (CSL). After centrifugation, counting, and assessment of viability by trypan blue exclusion, cells were stained as described. Data analysis was performed with the FlowJo Software (Tree Star). For cell sorting, single-cell suspensions were stained for CD11c, I-A/E, and B220 before sorting on an Epics Elite Flow Cytometer (Coulter). Sorted cell populations were either fixed for morphological studies or cultured for functional studies.

T cell stimulation assays

Single-cell suspensions obtained from DO11.10 mice lymph nodes were enriched for $CD4^+$ T cells to >95% purity with Dynabeads (Dynal). Before culturing, $CD4^+$ T cells were CFSE labeled (Molecular Probes), and 10^5 $CD4^+$ T cells per well were incubated with different ratios of sorted APC as indicated during 48 or 72 h in 96-well plates (200-μl volumes). OVA peptide 323–339 (OVA peptide; ISQAVHAAHAEINEAGR) was synthesized by Proteomics International (Perth, Australia), and whole OVA purchased from Sigma-Aldrich (OVA Grade IV); both were passaged over a polymyxin column (Detoxi-Gel; Pierce) to remove LPS. OVA peptide was added at a predetermined optimal concentration of 10 μg/ml. The following control cultures were systematically performed in parallel: 1) $CD4^+$ T cells only (no APC) in peptide containing medium, and 2) varying APC-to-T cell ratios in medium only (no peptide); background CD69 up-regulation was <5%, and cell division was <2%. To analyze in vitro T cell activation and proliferation, the following general gating strategy was used: a lymphocyte gate was set within the side-scatter vs forward-scatter profile, and $CD4^+$ cells were gated to examine CFSE dilution (proliferation) and/or CD69 expression (activation). Cells with the highest CFSE levels were undivided and defined the gate that was set to analyze $CD4^+$ T cell proliferation (i.e., cells with lower CFSE levels than the undivided cells peak on the histogram had undergone division and were therefore reported as percent divided of total $CD4^+$ T cells).

For the experiments using OVA protein, purified RT-DC (1×10^6/ml) were pulsed with 500 μg/ml OVA protein for 90 min at 37°C and washed before culture with CFSE-labeled DO11.10 $CD4^+$ T cells for 72 h as described above. Systematic control cultures consisted of 1) $CD4^+$ T cells (no APC) pulsed with protein, and 2) varying APC-to-T cell ratios in medium only (without protein); background CD69 up-regulation was <5% and cell division <2%.

Transmission electron microscopy

Cells sorted for TEM were prepared as previously described (16). Briefly, the sorted cells were immediately fixed in PBS containing 2.5% glutaraldehyde (EM grade; ProSciTech), before they were postfixed in an aqueous solution of 1% OsO_4 containing 1.5% $K_4Fe(CN)_6$. Subsequently, the cells were dehydrated and embedded into eppon. Ultrathin sections were stained with lead citrate and uranyl acetate and studied with JEOL2000 (Centre for Microscopy and Microanalysis, University of Western Australia).

APC turnover and in vivo Ag presentation studies

For APC turnover studies, naive animals were either lethally gamma irradiated using 11-Gy whole-body irradiation in two fractionated doses, or treated once with i.p. dexamethasone (10 mg/kg). Lung and tracheal tissue was then harvested at the indicated time points and prepared for flow-cytometric analysis as described above. For in vivo Ag presentation assays, wild-type BALB/c mice received 5×10^6 DO11.10 TCR transgenic lymph node cells i.v., labeled with CFSE according to method of Lyons and Parish (17) 3 days before intranasal (i.n.) inoculation with 100 μg of LPS-reduced OVA in 50 μl of pyrogen-free saline. RT-draining lymph nodes (DLN) (tracheobronchial (TBLN), posterior mediastinal (PMLN), and parathymic) were then harvested at the indicated time points and analyzed for CFSE and CD69 expression by KJ1-26^+CD4^+ cells as assessed by flow cytometry.

Statistics

Parametric statistical analysis of data was performed with Prism software (GraphPad Software) using the unpaired, nonparametric Student's t test. Values of $p < 0.05$ were considered statistically significant.

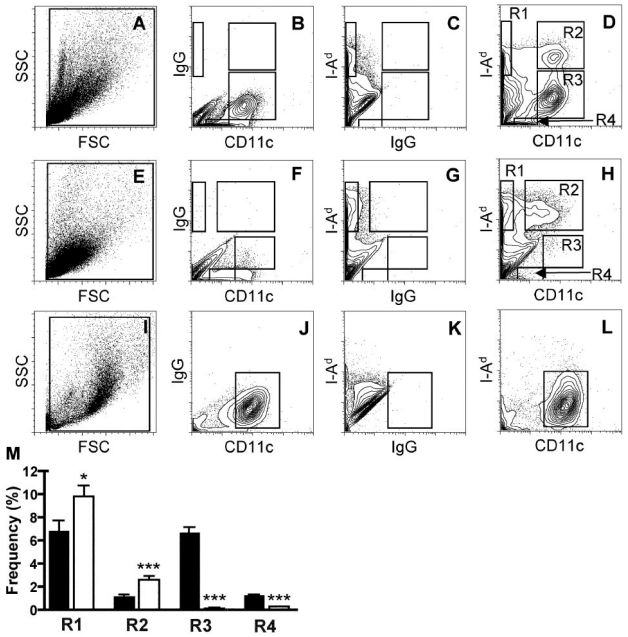

FIGURE 1. Flow-cytometric analysis and gating strategy for putative RT-APC. Total cells from lung parenchymal tissue (*A–D*), conducting airways (*E–H*), and BALF (*I–L*) were labeled with anti-mouse CD11c-PE and I-A^d-FITC (*D*, *H*, and *L*) or FITC-conjugated (*B*, *F*, and *J*) or PE-conjugated (*C*, *G*, and *K*) isotype control Igs. Gates were set for forward scatter (FSC) and side scatter (SSC) (*A*, *E*, and *I*) and appropriate gating regions set for each tissue site (R1–R4). *M*, Frequencies of RT-APC regions in different RT compartments expressed as a percentage of total cells for lung parenchyma (■) and main conducting airways (□). *, $p < 0.05$; ***, $p < 0.001$. Data are representative (*A–L*) or mean ± SEM (*M*) of eight experiments.

Results

Anatomical location within the RT determines the distribution of RT-APC subsets

To determine distribution of potential APC populations within different RT compartments, we compared flow-cytometric expression patterns of the prototypic APC markers CD11c and I-A^d on cells isolated from the lung parenchyma, the main conducting airways, and in BALF. Four distinct regions (R1–R4) were identified in parenchymal lung tissue digests (Fig. 1, *A–D*) based on the following characteristics: R1 cells were negative for CD11c and expressed high levels of I-A^d (CD11c^{neg}I-A$^{d\ high}$); R2 cells displayed high levels of both CD11c and I-A^d (CD11c^{high}I-A$^{d\ high}$); R3 cells also showed high levels of CD11c, but were highly autofluorescent and expressed low-to-negative levels of I-A^d (CD11c^{high}I-A$^{d\ low}$); R4 cells expressed intermediate levels of CD11c and were negative for I-A^d (CD11c^{int}I-A$^{d\ neg}$). Adopting a similar strategy for cells obtained from the main conducting airways revealed a markedly different CD11c and I-A^d profile, whereby this anatomical compartment was dominated by R1 and R2 cells (Fig. 1, *E–H*), with significantly reduced numbers of R3 ($p < 0.0001$) and R4 ($p < 0.0001$) cells compared with parenchymal lung tissue (Fig. 1*M*). Within BALF, the majority of cells (80.5 ± 6.7%) were highly autofluorescent, expressing high levels of CD11c and were low to negative for expression of I-A^d (Fig. 1, *I–L*).

Surface phenotype and ultrastructure identifies a RT-APC complexity not predicted by CD11c or I-A^d expression

To confirm that the classification of RT-APC populations defined above by surface phenotype defined subsets of cells with distinct morphologies, RT-APC populations from lung, airways, and BALF were sorted to high purity on the basis of the R1–R4 regions outlined in Fig. 1 and examined by TEM (Fig. 2). Lung parenchymal R1 cells uniformly displayed the characteristics of B cells as defined by size (diameter, 5–7 μm), scant cytoplasm, and a distinct nucleolus (Fig. 2*A*, arrowed). In contrast, R1 cells from the conducting airways consisted of a dominant population of B cells (Fig. 2*E*) and a minor population of cells with a mDC morphology (*F*). R2 cells of both the lung parenchyma (Fig. 2*B*) and conducting airways (*G*) consistently showed the typical ultrastructural features of mDC, including size (diameter, 10–14 μm), a lobulated nucleus, a distinct cytoskeleton, and abundant organelles. Lung parenchymal R3 cells exhibited the distinct morphological characteristics of mϕ, including size (diameter, 8–10 μm) and abundant phagocytosed material in distinct phagolysosomes (Fig. 2*C*, arrowed) similar to alveolar mϕ obtained from BALF (*H*). Lung parenchymal R4 cells were comprised principally of a DC/monocytic precursor cell type (Fig. 2*D*), consistent with the observation that purified cells from this region gave rise to cells with the phenotypic characteristics of lung parenchymal R1–R4 after overnight culture in GM-CSF (data not shown).

We next performed a detailed analysis of the cell surface phenotype of populations of cells within R1–R4 of lung, airways, and BALF, using an extensive panel of lineage, differentiation, and costimulatory markers (Fig. 3). Cells within each of the gated regions expressed a characteristic set of markers that was consistent with their cellular morphology summarized as follows: A high

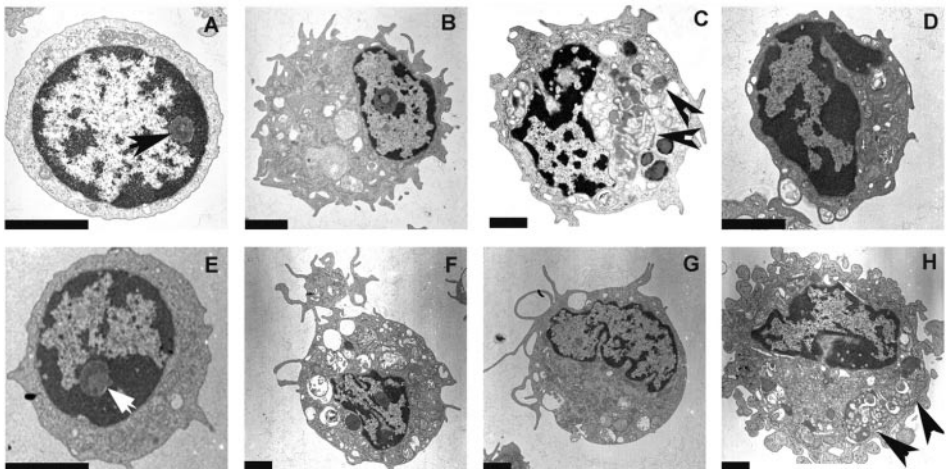

FIGURE 2. TEM images of sorted RT-APC populations. Lung parenchyma, conducting airways tissue digests, and BALF were sorted according to the regions identified in Fig. 1 and processed for TEM. *A–D*, Lung parenchymal R1 B cells (*A*), R2 mDC (*B*), R3 mø (*C*), and R4 monocytic precursor cells (*D*). *E–G*, Conducting airway R1 B cells (*E*), R1 mDC (*F*), and R2 mDC (*G*). *H*, BALF alveolar mø. Nucleoli (*A* and *E*) and phagolysosomes (*C* and *H*) are indicated by arrowheads. Bars, 2 μm.

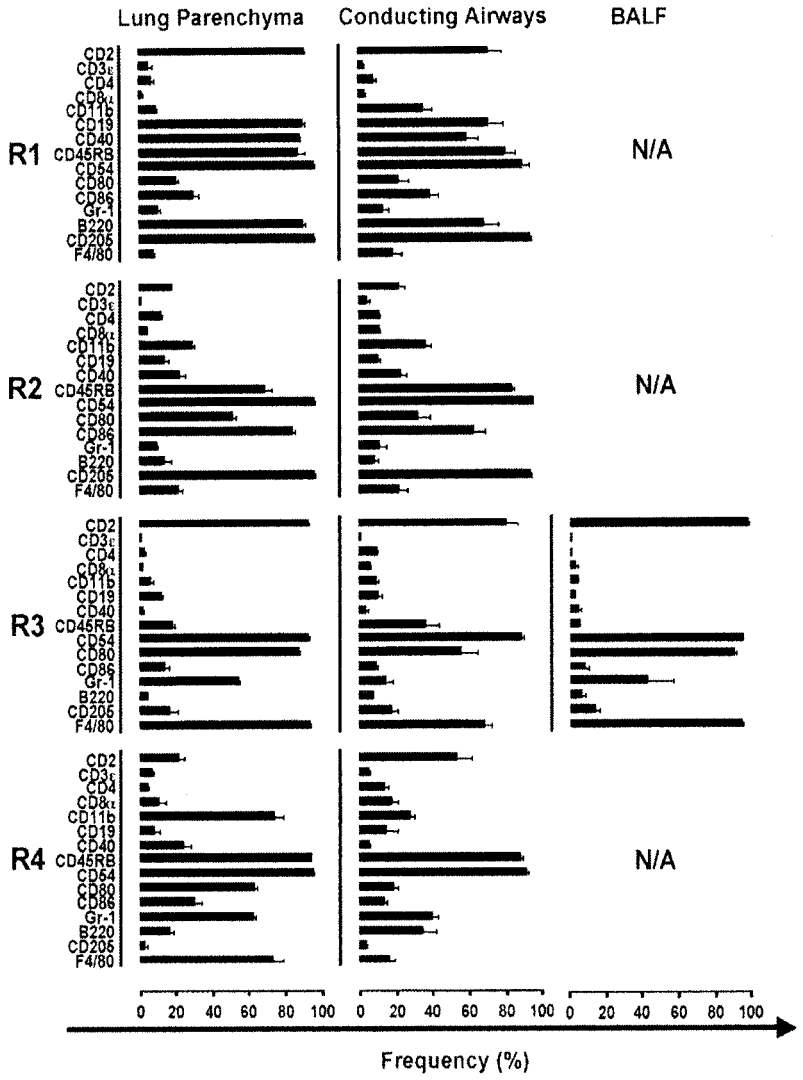

FIGURE 3. Analysis of surface marker expression by RT-APC subsets. Lung, airway, and BALF cells were labeled with CD11c-PE, I-A^d-FITC, and biotinylated mAbs to the indicated cell surface markers followed by streptavidin-PE/Cy5. R1–R4 were gated as described in Fig. 1, and the expression of each marker was determined based on gates set on appropriate isotype controls. Data are means ± SEM of three to eight experiments expressed as a percentage frequency of expression after subtraction of background staining of isotype control Abs within each region. N/A, Not applicable.

proportion (>90%) of R1 cells expressed CD2, CD19, B220, and CD205, which, together with the morphological data described above, was consistent with these being mature B cells; R2 cells expressed CD11b and CD205 and the majority (>80%) also expressed CD86 and lower frequencies (>50%) of CD80, consistent with an mDC phenotype; the majority (>90%) of R3 cells in lung parenchyma expressed CD54, CD80, and F4/80, consistent with a mϕ phenotype. This was also the case for analysis of parenchymal lung tissue R3 cells following extensive lavage, suggesting these to be resident tissue mϕ (data not shown); R4 cells expressed CD45RB and CD54 at high frequencies (>90%), and CD11b, CD80, Gr-1, and F4/80 at lower frequency (>50%) and consistent with a myeloid origin for these cells.

Similar expression profiles were observed for the populations within the main conducting airways, the principal difference at this site being a higher frequency of B220$^-$ cells in R1 (Fig. 3). Furthermore, expression of CD4 and CD8α (as described on lymph node DC subsets (11)) were low to negative in all regions analyzed. A summary of the defining cell surface marker characteristics of each RT-APC subset is shown in Fig. 4 and Table I. Finally, staining with the 120G8 mAb specific for mouse pDC (13) showed a small percentage of typical CD11c^{int}I-A$^{d\ int}$120G8^{pos} pDC in the lung parenchyma (0.15%) and main conducting airways (0.27%) and more prominent populations of CD11c^{neg}120G8^{pos} cells that expressed lower levels of I-A^d in both sites that did not conform to the phenotype previously described for pDC in lymph nodes (13) (data not shown).

Functional characterization defines a high degree of heterogeneity among steady-state RT-APC subsets

Given the heterogeneity in APC population distribution between RT sites identified above, we next sought to determine whether this also represented heterogeneity at the functional level. As an initial measure of functional activity, mannose receptor-mediated endocytic uptake of 40-kDa DX-FITC by ex vivo RT-APC subsets was assessed. Both lung parenchymal mDC (R2) and mϕ (R3) were highly endocytic, reaching peak uptake activity at 30 min of incubation, after which time uptake levels began to decline (Fig. 5*A*). In contrast, the multipotential precursor population (R4) was weakly endocytic, whereas lung B cells (R1) were nonendocytic (Fig. 5*A*). Similarly, mDC (R2) of the main conducting airways were also highly endocytic, whereas all R1 cells (B cells and mDC) from this site were nonendocytic (Fig. 5*B*). Furthermore, although showing slower uptake kinetics, the endocytic capacity of airway mDC was ultimately greater than their lung counterparts, as indicated by higher levels of DX-FITC uptake (data not shown) and proportion of endocytic cells at late time points (>90 min) (data not shown).

Next, to determine the CD4$^+$ T cell-stimulating capacity of each RT-APC subset, we examined the ability of purified populations to present an I-A^d-restricted OVA-peptide to naive OVA-specific

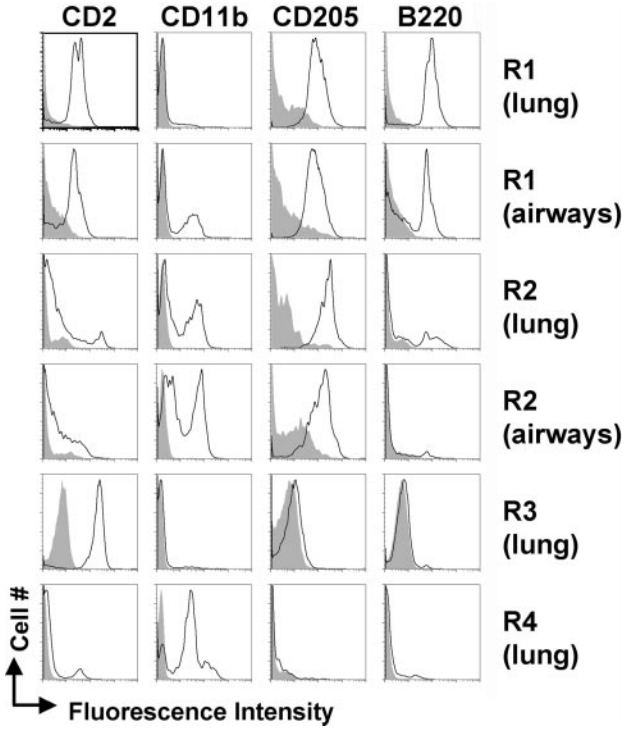

FIGURE 4. Selected surface marker expression by RT-APC subsets. Cells were isolated from lung parenchymal or conducting airway tissue, labeled with CD11c, I-A^d, and the indicated surface markers, and analyzed by flow cytometry. Gates were set for R1–R4 as described in Fig. 1, and the expression of the indicated surface markers was then analyzed within each region (dark lines) and compared with an appropriate isotype control IgG (filled histograms). Data are shown for a representative of eight experiments.

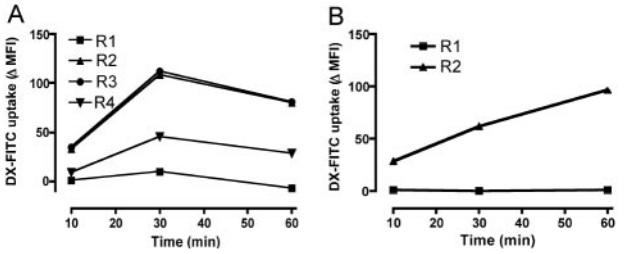

FIGURE 5. Ex vivo endocytotic capacity of RT-APC from lung and conducting airways. Total lung parenchyma (*A*) and conducting airways (*B*) were labeled for CD11c and I-A^d and then incubated for the indicated length of time with DX-FITC at either 4 or 37°C. At the end of each time period, the reaction was stopped by washing in cold buffer, and DX-FITC uptake was determined in each tissue region (as defined in Fig. 1) by flow cytometry. Data are expressed as a ΔDX-FITC uptake at 37°C obtained by subtraction of 4°C control values, and the data shown are representative of a series of three experiments.

TCR transgenic CD4$^+$ T cells in vitro (Fig. 6). Both lung parenchymal B cells (R1) and mDC (R2) were potent stimulators of naive CD4$^+$ T cells, inducing significant up-regulation of CD69 after 48 h (Fig. 6*A*) and T cell proliferation after 72 h (*C*) compared with mø (R3). Whereas both lung parenchymal B cells (R1) and mDC (R2) stimulated strong T cell proliferation at high APC:T cell ratios (Fig. 6*C*; 1:10), the immunostimulatory capacity of B cells was significantly weaker than that of mDC at lower ratios (Fig. 6*C*; 1:100). In contrast, while lung R4 cells induced low-level CD69 up-regulation on T cells at 48 h of culture (Fig. 6*A*), this population did promote strong T cell division at 72 h (*C*). Further analysis revealed that in R4-stimulated cultures CD69 up-regulation on T cells was delayed until 72 h, suggesting that R4 cells required maturation and/or differentiation during the culture period to achieve full immunostimulatory capacity (Fig. 6*E*). In contrast, lung parenchymal mϕ (R3) did not induce CD69 expression or T cell proliferation at any APC:T cell ratio (Fig. 6, *A* and *C*). Furthermore, CD4$^+$ T cell proliferation was substantially reduced in cultures where total CD11c^{high} cells from parenchymal lung tissue were used as APC compared with those where the R3 mϕ population had been removed, indicating a potential suppressive activity for this subset of cells (data not shown).

Within the conducting airways, mDC (R2) were highly immunostimulatory, inducing CD69 expression at 48 h (Fig. 6*B*) and a level of CD4$^+$ T cell proliferation at 72 h (*D*) that was consistently of a greater magnitude than their lung parenchymal counterparts (*A* and *C*). Total R1 cells from the conducting airways, which consisted of both a dominant B cell and minor CD11c^{neg} mDC population, were less effective than R2 mDC at inducing CD69 expression at 48 h (Fig. 6*B*) and T cell proliferation at 72 h of culture (*D*). When this region was sorted on the basis of B220 expression, B220^{neg} mDC induced significantly lower levels of CD69 up-regulation at 48 h (Fig. 6*B*) and T cell proliferation at 72 h (*D*) than B220^{pos} B cells from the same region or mDC from R2. Again, as described for lung R4 cells (Fig. 6*E*), B220^{neg} mDC within R1 of the conducting airways induced a delayed up-regulation of CD69 on T cells (*F*).

Steady-state mDC from lung and airways show a poor capacity to process intact protein for presentation to naive CD4$^+$ T cells

The strong capacity for mDC from lung and conducting airways to stimulate naive CD4$^+$ T cell proliferation in response to OVA peptide was not expected, given our previous rat studies suggesting that ex vivo steady-state RT-DC have a poor Ag-presenting capacity unless given a maturation stimulus in vitro (15). Furthermore, although a high proportion of mDC expressed the costimulatory molecule CD86, and to a lesser extent CD80 and CD40 (see Fig. 3), the intensity of expression of these molecules was relatively low ex vivo compared with the up-regulation achieved following overnight maturation in rGM-CSF, suggesting that mouse RT-DC are only partially matured in the steady state (data not

Table I. *Summary of RT-APC phenotypic characteristics*[a]

Region	Cell Type	CD11c	I-A^d	CD2^{high}	CD11b	CD205	B220
1	B cell[b]	−	+++	+++	+	+++	+++[b]
2	mDC	+++	+++	±	+	+++	±
3	mϕ	+++	±	+++	−	+	−
4	Pre-DC	+	−	+[c]	+++	−	±

[a] −, <10%; ±, 11–20%; +, 21–40%; ++, 41–60%; +++, >61%.
[b] Additional B220$^-$ DC population in the main conducting airways.
[c] ++ in main conducting airways.

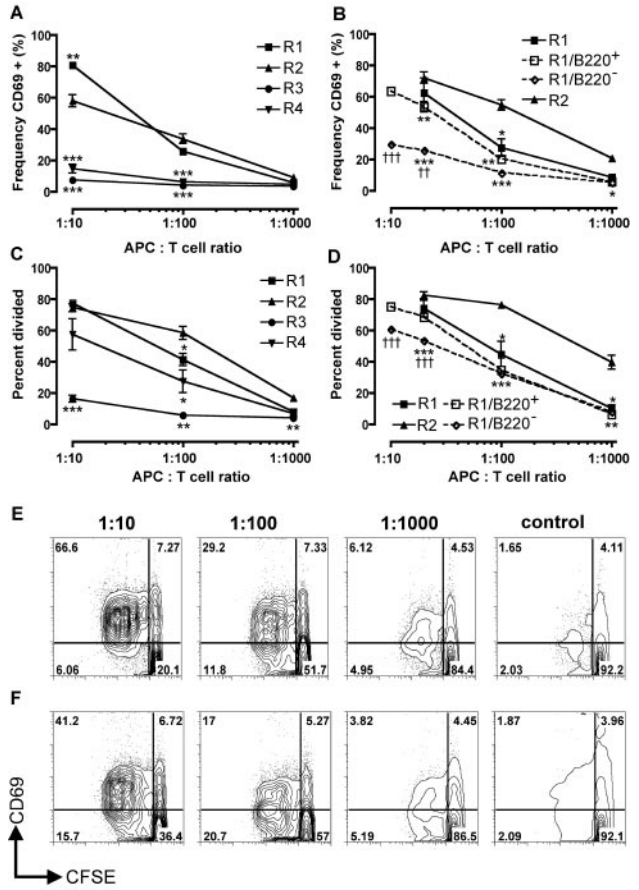

FIGURE 6. In vitro OVA-specific $CD4^+$ T cell activation induced by ex vivo-derived RT-APC populations from lung and conducting airways in response to OVA peptide. APC populations were purified by cell sorting according to the gating strategy outlined in Fig. 1 and incubated ex vivo at varying ratios with CFSE-labeled $CD4^+$ T cells from DO11.10 mice in medium containing 10 μg/ml OVA peptide. Early T cell activation was examined by expression of CD69 on OVA-specific KJ1-26^+CD4^+ T cells at 48 h of culture (*A* and *B*), and T cell division was determined by calculating the proportion of $CD4^+$ T cells entering division as assessed by sequential loss of CFSE staining at 72 h of culture (*C* and *D*) for lung parenchyma (*A* and *C*) and conducting airways (*B* and *D*). CD69 expression on dividing cells was also examined at 72 h of culture in cultures stimulated by lung parenchymal R4 cells (*E*) and conducting airway R1 $B220^-$ cells (*F*). *, $p < 0.05$; **, $p < 0.001$; ***, $p < 0.0001$ vs R2. ††, $p < 0.001$; †††, $p < 0.0001$ main conducting airways R1 $B220^+$ vs R1 $B220^-$. Data are representative of a series of at least three experiments and expressed as mean ± SEM of at least three experiments.

shown). Therefore, in the current study, we sought to determine whether the high immunostimulatory capacity of mouse DC for "preprocessed" peptide loaded directly onto MHC extended to their capacity to process and load peptide from intact proteins. To address this, a similar range of T cell-activating studies were performed, this time using purified mDC pulsed with whole, LPS-reduced OVA for 90 min in vitro before culture with naive, OVA-specific $CD4^+$ T cells (Fig. 7). In contrast to peptide, steady-state mDC from both lung and airways showed a poor capacity to process and present whole OVA protein to naive $CD4^+$ T cells (Fig. 7). However, when the cells were matured in GM-CSF after OVA pulsing but before addition to $CD4^+$ T cells, then mDC from both sites showed potent T cell-stimulating activity (Fig. 7), confirming that steady-state RT-DC are functionally immature.

Immunostimulatory RT-APC subsets have a short half-life in tissue, correlating with a rapid translocation of Ag signaling to DLNs

As proposed by us (6) and others (18), a key feature of immune surveillance at respiratory and other mucosal surfaces is the rapid transmission of antigenic signals to lymph nodes for scrutiny by the recirculating naive T cell pool. We therefore investigated the relative turnover rates of each of the RT-APC subsets at each anatomical location by determining their depletion kinetics following lethal gamma irradiation in addition to depletion and repopulation kinetics following high-dose systemic dexamethasone administration. Twelve to 24 h after gamma irradiation, lung parenchymal B cells (R1), mDC (R2), and R4 cells were reduced to <50% of their initial starting frequencies (Fig. 8*A*). Similarly, conducting airway R1 cells (B cells and $CD11c^{neg}$ mDC) and $CD11c^{pos}$ mDC (R2) showed rapid depletion kinetics following lethal gamma irradiation (Fig. 8*B*). In contrast, lung parenchymal mϕ (R3) were long-lived, with decreases only apparent 7 days postirradiation (Fig. 8*A*). Similar depletion rates for all populations were also observed following high-dose systemic dexamethasone administration, confirming that these effects were not due to the toxic effects of whole-body irradiation (Fig. 8, *C* and *D*). In addition, the repopulation rates of each region at later time points following dexamethasone metabolism and bone marrow regeneration were consistent with the rapid turnover rates (<24 h) of B cells, mDC, and pre-DC in lung parenchyma and conducting airways and much slower turnover rates (>7 days) of lung parenchymal mϕ (Fig. 8, *C* and *D*). In summary, these data demonstrate that those populations of RT-APC defined as possessing a moderate-to-high immunostimulatory capacity (mDC, B cells, and including R4 multipotential precursors) showed short tissue half-lives, whereas those with weak immunostimulatory activity (i.e., lung mϕ) were much longer-lived.

The data above indicated that uptake of Ag in the RT by immunostimulatory APC, and more specifically RT-DC, should lead to a rapid translocation (<12 h) of antigenic signals via the afferent lymphatics to local DLNs. To confirm that this was the case, an in vivo time course of CD69 up-regulation on adoptively transferred, naive $CD4^+$ OVA-specific TCR transgenic T cells was analyzed in DLNs at early time points following a single i.n. inoculation of LPS-reduced OVA. By this method, activation of $CD4^+$ T cells in DLNs (PMLN, TBLN), but not nondraining lymph nodes (inguinal lymph nodes (ILN)), was first apparent 6 h, with a peak at 12–18 h, following i.n. administration of OVA (Fig. 9), thus matching the rapid turnover rates observed for immunostimulatory RT-APC populations (see Fig. 8). Furthermore, our preliminary data suggests that the rapid translocation of Ag to the DLN is restricted predominantly to a $CD11c^{high}I\text{-}A^{d\ high}CD11b^{high}$ mDC (C. von Garnier, E. Batanero, M. Wikstrom, M. Smith, P. Holt, and P. A. Stumbles, manuscript in preparation).

Discussion

Due to their potent immunoregulatory capacity, RT-DC have been the focus of intense research, more recently as potential targets for the immunotherapy of allergic airways disease. The RT consists of a number of distinct microanatomical compartments, exemplified by the differences between the mucosal tissues of the conducting airways and parenchymal tissues of the alveolar regions. It is now recognized that the function(s) of DC are modulated by factors generated in their host tissue, and it is accordingly likely that DC populations resident within different tissue microenvironments within the RT will be differentially regulated. To date, however, a systematic characterization of APC populations and DC subsets present within the different tissue compartments of the RT has not been undertaken. Most studies have focused on the analysis of

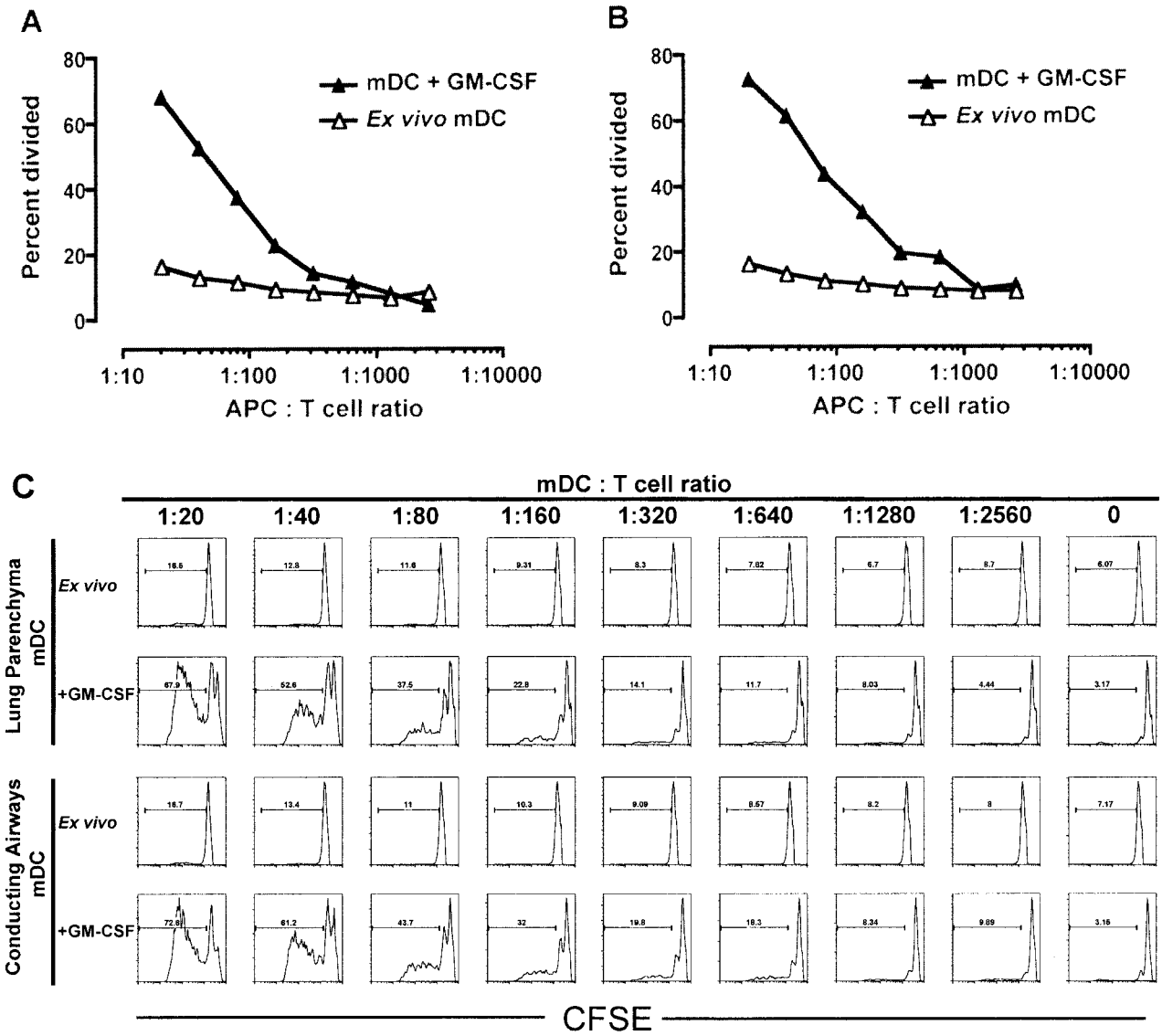

FIGURE 7. In vitro OVA-specific $CD4^+$ T cell activation induced by ex vivo-derived or GM-CSF-matured mDC in response to whole OVA protein. R2 mDC were sorted from lung parenchyma (*A*) and conducting airways (*B*) tissue digests according to the gating strategy outlined in Fig. 1 and pulsed for 90 min with 500 μg/ml LPS-reduced OVA prior and then washed in complete medium. OVA-pulsed mDC were then incubated without further manipulation (ex vivo), or following overnight incubation with 20 ng/ml recombinant mouse GM-CSF, for 72 h with CFSE-labeled $CD4^+$ T cells from DO11.10 mice. Results are expressed as percentage of OVA-specific KJ1-26^+CD4^+ T cells that had entered one or more divisions as assessed by sequential loss of CFSE staining. One representative experiment of two is shown. *C*, In vitro OVA-specific $CD4^+$ T cell activation induced by ex vivo-derived or GM-CSF-matured mDC in response to whole OVA protein. Histograms show the percentage of OVA-specific $CD4^+$ T cells that had entered one or more divisions as assessed by sequential loss of CFSE staining. One representative experiment of two is shown.

whole-lung tissue preparations under the assumption that APC and DC distribution will be uniform throughout the tissue. In this study, we report a comprehensive series of analyses of RT-APC and DC distribution within different anatomical compartments of the RT, which demonstrate that this assumption is incorrect: our data reveal a high degree of hitherto-unrecognized complexity in relation to distribution and function of the different RT-APC populations.

Our initial analyses aimed to determine the distribution of expression of the prototypic DC marker CD11c within the two major compartments of the RT, namely, the main conducting airways and parenchymal lung, as being representative of local mucosal and parenchymal tissue compartments, respectively. Analysis of CD11c in conjunction with $I\text{-}A^d$ expression on cell preparations from both of these sites revealed a unique pattern of expression for both markers. Of note was the identification of at least three distinct populations of CD11c-expressing cells in lung tissue that differed in their levels of $I\text{-}A^d$ expression (R2–R4; Fig. 1), suggesting that expression of CD11c was not unique to DC in lung tissue. This was confirmed by further cell surface phenotypic studies, which revealed differential expression of a number of APC "lineage" markers such as B220, CD205, and CD11b among CD11c-expressing populations of lung tissue. In conjunction with a series of detailed ultrastructural studies performed on purified populations of cells, we confirmed that high-level CD11c expression, in addition to expression on mDC, is also associated with a predominant population of autofluorescent mϕ that were negative for CD11b and expressed low levels of $I\text{-}A^d$, consistent with other recent studies in this area (19–21). In addition, peripheral lung mϕ also uniformly expressed high levels of CD2 (Fig. 3). CD2 is a member of

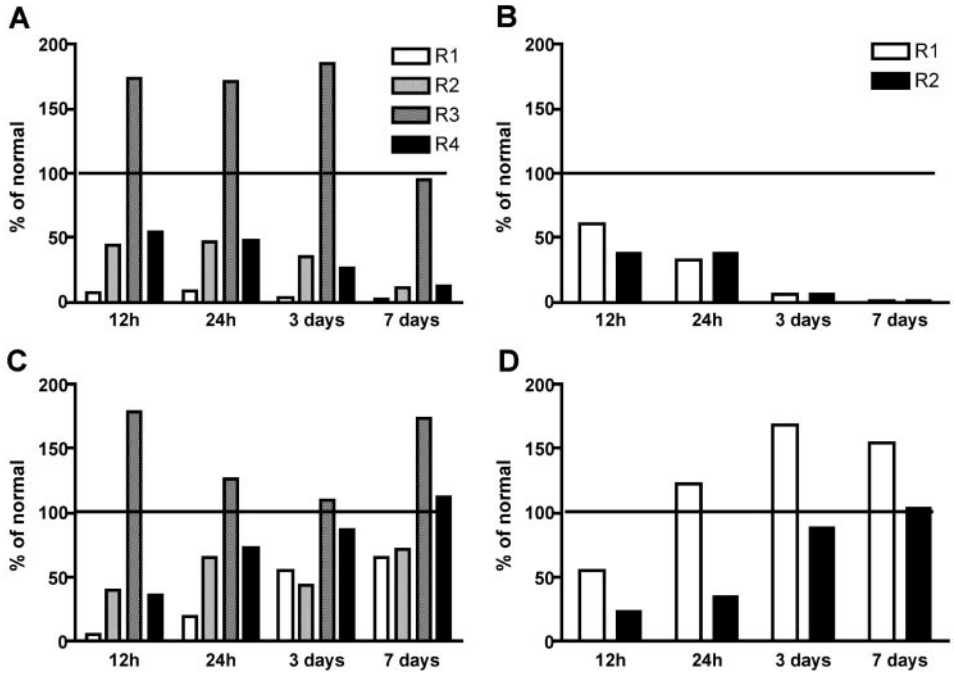

FIGURE 8. Depletion kinetics of RT-APC populations. Mice received either split-dose whole-body gamma irradiation (*A* and *B*) or i.p. dexamethasone (10 mg/kg) (*C* and *D*) at the indicated times before isolation of lung parenchyma (*A* and *C*) and conducting airways (*B* and *D*) for phenotyping. The time courses were repeated twice with similar results. Regions are as defined in Fig. 1, and results are expressed as percentage change from normal population frequencies.

the Ig superfamily that binds CD48 in mice, the binding of which lowers the threshold for activation of T cells by Ag (22). Early studies described expression of CD2 on rat splenic mϕ (23); however, to our knowledge, this is the first description of expression of this molecule on mouse RT mϕ. Although the function of CD2 on mϕ is unknown, it may play a role in mediating cell-cell interactions between mϕ and other cell types that express CD48, such as DC (24). In this respect, the presence of mϕ within the lung parenchymal compartment may potentially affect local immunological homeostasis, because this type of APC has been shown to profoundly inhibit T cell responses to Ag presented by RT-DC in the rat (25), and we have preliminary data to suggest this is also the case for mouse (data not shown). This suppressive activity could be overcome by GM-CSF (9), a well-described murine RT-DC maturation factor (15), and was mediated by mϕ-derived NO that both prevented RT-DC maturation and inhibited T cell activation by disruption of Jak3/STAT5-dependent IL-2R signaling (8, 26). Other locally produced factors that are known to modulate DC activity include mediators such as TNF-α, IL-1, TGFβ, IFN-γ, and PGE_2 (9, 27, 28), surfactant proteins (29), and corticosteroids, as shown in our turnover experiments and previous studies (30–32). Hence, the T cell stimulation activity of RT-DC is under tight microenvironmental control in lung tissue, which under normal circumstances would restrain local T cell activation and hence tissue inflammation. Finally, lower levels of CD11c were also expressed on a myeloid precursor population with APC potential in lung tissue (Fig. 1, region 4, and Fig. 6, *A*, *C*, and *E*). Our preliminary data suggest that this population is capable of developing into the major APC subsets of lung tissue, including mDC, following differentiation in vitro (D. Strickland, C. von Garnier, M. Wikstrom, M. Smith, P. Holt, and P. A. Stumbles, manuscript in preparation).

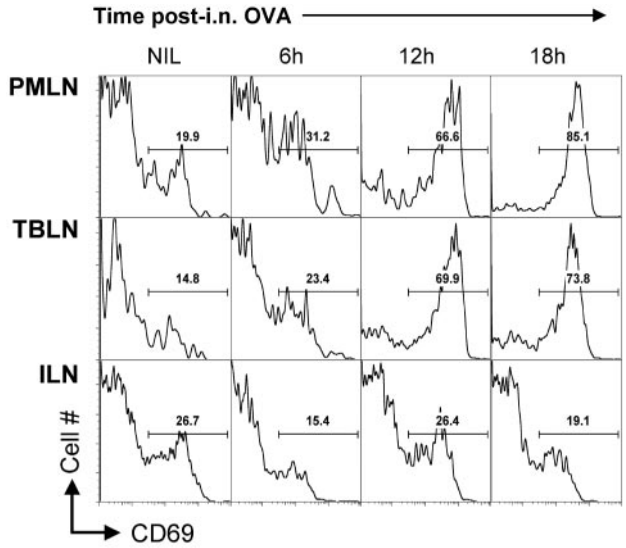

FIGURE 9. Time course of in vivo activation of OVA-specific $CD4^+$ T cells in DLNs following exposure to i.n. OVA. Mice were inoculated i.n. with 100 μg of OVA in 50 μl of saline 2 days after adoptive transfer of CFSE-labeled $CD4^+$ T cells from DO11.10 donors. Draining PMLN and TBLN and nondraining ILN were pooled from groups ($n = 5$) of nonexposed mice or mice 6, 12, and 18 h after OVA inoculation, and CD69 expression on OVA-specific KJ1-26^+CD4^+ T cells was analyzed. Analysis gates were set based on isotype control IgG staining, and the experiment was performed twice with similar results.

In contrast to lung tissue, CD11c expression in the main conducting airways showed a more restricted pattern of expression, being principally confined to $CD11c^{high}$I-$A^{d\ high}CD205^{high}$ mDC in this site. Although mϕ are known to be present in, or recruited to, airway mucosal tissue (33), the absence of a significant population of $CD11c^{high}CD2^{high}$ mϕ at this site raises the possibility that airway DC are not under the same degree of local immunosuppression as may be the case for their lung tissue counterparts. Indeed, this appeared to be the case in terms of Ag uptake capacity, where conducting airway DC showed a greater capacity for mannose receptor-mediated endocytosis compared with lung tissue DC. Additionally, conducting airway DC also showed an enhanced capacity for peptide Ag loading and presentation to naive $CD4^+$ T cells. Our data for B cells from both sites (which were nonendocytic but efficiently presented peptide Ag) indicated that peptide-presenting activity was independent of endocytic capacity, thus suggesting an intrinsic capacity for enhanced Ag presentation by

airway DC. Finally, our data showing very low levels of expression of the pDC marker 120G8 among CD11c-expressing populations in both tissue sites (airway and lung) suggested that this subset of DC does not constitute a significant population of cells within the mouse RT. Furthermore, costaining with B220, another putative pDC marker, together with additional mouse B cell markers (CD19 and CD2 (34)) suggested that any B220 expression within CD11c-expressing populations could be accounted for by in situ or ex vivo clustering with B cells, an event also confirmed by TEM (data not shown). Additionally, the other major population of B220-expressing cells (R1 in lung and conducting airways) was confirmed by phenotype ($CD19^+B220^+CD2^+I\text{-}A^{high}$) and morphology to be mature B cells, with no morphological evidence of pDC in this region. Interestingly, B cells of the RT also expressed high levels of the putative DC marker CD205 (DEC-205). Although it is possible that DEC-205-expressing B cells may be represented at with higher frequency in the RT due to environmentally driven recruitment or up-regulation of this marker, this phenotype is not unique to the RT because expression of DEC-205 on mature populations of B cells has been previously described on mouse B cells from other tissues sites (35, 36). These data provide further evidence that a multiparameter approach is required for the definition of DC and other APC types within the mouse RT.

Given that the in situ Ag-presenting activity of RT-DC in airways must be under tight regulation to avoid local immunopathology, we were interested to determine at what level this control may be operating. DC maturation is thought to lead to phenotypic changes that correlate with an increased capacity for Ag processing and T cell activation (37). These phenotypic alterations include enhanced synthesis of MHC-peptide complexes, enhanced T cell binding, expression of costimulatory surface molecules, and production of chemokines (38), cytokines (39), and growth factors (40, 41). Previously, our work on RT-DC in the rat showed that expression of costimulatory molecules such as CD80 and CD86 is low under noninflammatory conditions, indicating that this may represent a mechanism of functional regulation of RT-DC maturity in this species (15). However, our current data on mouse RT-DC indicated that CD86 and, to a lesser extent, CD80 and CD40, were constitutively expressed by a significant number of RT-DC in the steady state. However, the intensity of expression of these molecules was relatively low when compared with the levels achieved following maturation in GM-CSF, consistent with the rat data suggesting that RT-DC are relatively immature in situ and indicating that the peptide response is either relatively independent of costimulation or that these molecules are rapidly up-regulated during the period of culture with peptide-stimulated $CD4^+$ T cells.

However, in contrast to peptide presentation, the capacity of RT-DC populations to process and present whole protein Ag was distinctly suppressed. Although the mechanisms for controlling this process in vivo remain unclear, these data suggest that resident tissue RT-DC are able to rapidly present free processed peptides in their local tissue microenvironment to recirculating T cells (Fig. 5), but the capacity to process and present whole protein Ags is confined to mature cells (Fig. 6) or Ag-bearing cells entering the DLNs (Fig. 8). This may represent a potential mechanism for rapid local tissue memory T cell activation by pathogen-derived peptides released by local phagocytes, which our group and others have shown to be recruited into the airway mucosa during acute inflammatory responses (30), while restricting naive T cell activation to whole protein Ags to DLNs.

In mouse lymphoid tissue, at least five subsets of DC have been described based on expression of markers including MHC class II, CD11b, CD205, CD4, and CD8 (11). However, in the mouse RT, we found a very limited number of subsets, principally $CD4^-CD8^-CD11b^+CD205^+$ "myeloid" DC, with no evidence of $CD8\alpha^+$ DC or so-called CD4 CD8 double-negative DC. This DC subpopulation was found to contain high levels of i.n. administered OVA-Alexa 488 in both the RT and DLN, and based on kinetic studies, this population is the most likely DC involved in Ag trafficking from the RT to the DLN (C. von Garnier, E. Batanero, M. Wikstrom, M. Smith, P. Holt, and P. A. Stumbles, manuscript in preparation). Additionally, we also found a small population of $CD11c^{int}I\text{-}A^{d\ low}120G8^{pos}$ cells, consistent with the phenotype described for mouse pDC (13), in lung tissue and conducting airways. An additional and prominent population of $CD11c^{neg}120G8^{pos}$ cells was also observed in both lung and airways, which did not fit the typical staining pattern described for pDC in lymph nodes (13) and which at this stage remain undefined. However, in contrast to the results of De Heer et al. (42), our preliminary data suggest that only mDC, and not $120G8^{pos}$ pDC, mediate traffic of OVA to DLN following i.n. OVA exposure (C. von Garnier, E. Batanero, M. Wikstrom, M. Smith, P. Holt, and P. A. Stumbles, manuscript in preparation).

B cells were also a dominant population present in both anatomical locations and were capable of inducing a similar T cell activation to DC at high APC-to-T cell ratios. This finding contrasts with results from previous studies by Masten and Lipscomb (7), which found lung B cells to have a diminished capacity to present Ag due to decreased levels of both MHC class II and costimulatory molecules. The observation that DC and B cells coexist in the RT may have relevant functional consequences, because DC have been shown to transfer Ag directly to B cells, thereby initiating class switching (43). Therefore, the potential for interaction of these two APC types within both RT compartments may profoundly affect local humoral and cellular immunity. Indeed, lymphoid follicles containing B cells have been shown to be present in the airways under pathological conditions, such as asthma and exposure to tobacco smoke (44), and were associated with airway wall inflammation and remodeling.

Finally, turnover rates of RT-DC populations determined in our earlier studies in the rat indicated that these varied throughout the RT, with the DC turnover time in the main conducting airways being in the order of 3 days for 85% of the population (coexisting with a minor subset of long-lived cells), and ~10 days for lung parenchymal DC (45). In the current study, similar experiments performed in the mouse indicated an even more rapid steady-state turnover with half-lives of <12 h for most RT-DC throughout the entire RT, again coexisting with a minor subset of long-lived cells. The observation of exceptionally rapid turnover rates for RT-DC populations in the mouse is thus far unique to this species. Our earlier studies in the rat (33, 46) and humans (47) indicated that this turnover is driven by inhaled irritant (and/or antigenic) stimuli. The exceptional rapidity of this process in the mouse again may be driven by environmental stimuli and may also be a reflection of the high resting respiratory rate in this species, which would result in highly efficient sampling of airborne particles. Whether these species differences have consequences in relation to the functional phenotype of respective RT-DC populations remains to be established. Additionally, whether the longevity of parenchymal lung mϕ populations has functional consequences for local immunity by regulating RT-DC function and/or retaining Ag for extended periods of time is currently the focus of further studies.

Acknowledgments

We thank M. Erni and Gery Barmettler (Institute of Anatomy, University of Zurich, Zurich, Switzerland) for assistance with the preparation of cells for TEM. The TEM specimens were analyzed and documented at the Centre for Microscopy and Microanalysis (University of Western Australia).

Disclosures

The authors have no financial conflict of interest.

References

1. Sedgwick, J. D., and P. G. Holt. 1983. Induction of IgE-isotype specific tolerance by passive antigenic stimulation of the respiratory mucosa. *Immunology* 50: 625–630.
2. Tsitoura, D. C., R. H. DeKruyff, J. R. Lamb, and D. T. Umetsu. 1999. Intranasal exposure to protein antigen induces immunological tolerance mediated by functionally disabled $CD4^+$ T cells. *J. Immunol.* 163: 2592–2600.
3. Brimnes, M. K., L. Bonifaz, R. M. Steinman, and T. M. Moran. 2003. Influenza virus-induced dendritic cell maturation is associated with the induction of strong T cell immunity to a coadministered, normally nonimmunogenic protein. *J. Exp. Med.* 198: 133–144.
4. Lambrecht, B. N., and H. Hammad. 2003. Taking our breath away: dendritic cells in the pathogenesis of asthma. *Nat. Rev. Immunol.* 3: 994–1003.
5. Holt, P. G., and P. A. Stumbles. 2000. Regulation of immunologic homeostasis in peripheral tissues by dendritic cells: the respiratory tract as a paradigm. *J. Allergy Clin. Immunol.* 105: 421–429.
6. Stumbles, P. A., J. W. Upham, and P. G. Holt. 2003. Airway dendritic cells: co-ordinators of immunological homeostasis and immunity in the respiratory tract. *APMIS* 111: 741–755.
7. Masten, B. J., and M. F. Lipscomb. 1999. Comparison of lung dendritic cells and B cells in stimulating naive antigen-specific T cells. *J. Immunol.* 162: 1310–1317.
8. Holt, P. G., J. Oliver, N. Bilyk, C. McMenamin, P. G. McMenamin, G. Kraal, and T. Thepen. 1993. Downregulation of the antigen presenting cell function(s) of pulmonary dendritic cells in vivo by resident alveolar macrophages. *J. Exp. Med.* 177: 397–407.
9. Bilyk, N., and P. G. Holt. 1993. Inhibition of the immunosuppressive activity of resident pulmonary alveolar macrophages by granulocyte/macrophage colony-stimulating factor. *J. Exp. Med.* 177: 1773–1777.
10. Strickland, D. H., T. Thepen, U. R. Kees, G. Kraal, and P. G. Holt. 1993. Regulation of T-cell function in lung tissue by pulmonary alveolar macrophages. *Immunology* 80: 266–272.
11. Shortman, K., and Y. J. Liu. 2002. Mouse and human dendritic cell subtypes. *Nat. Rev. Immunol.* 2: 151–161.
12. Asselin-Paturel, C., A. Boonstra, M. Dalod, I. Durand, N. Yessaad, C. Dezutter-Dambuyant, A. Vicari, A. O'Garra, C. Biron, F. Briere, and G. Trinchieri. 2001. Mouse type I IFN-producing cells are immature APCs with plasmacytoid morphology. *Nat. Immunol.* 2: 1144–1150.
13. Asselin-Paturel, C., G. Brizard, J. J. Pin, F. Briere, and G. Trinchieri. 2003. Mouse strain differences in plasmacytoid dendritic cell frequency and function revealed by a novel monoclonal antibody. *J. Immunol.* 171: 6466–6477.
14. Anjuere, F., P. Martin, I. Ferrero, M. L. Fraga, G. M. del Hoyo, N. Wright, and C. Ardavin. 1999. Definition of dendritic cell subpopulations present in the spleen, Peyer's patches, lymph nodes, and skin of the mouse. *Blood* 93: 590–598.
15. Stumbles, P. A., J. A. Thomas, C. L. Pimm, P. T. Lee, T. J. Venaille, S. Proksch, and P. G. Holt. 1998. Resting respiratory tract dendritic cells preferentially stimulate T helper cell type 2 (Th2) responses and require obligatory cytokine signals for induction of Th1 immunity. *J. Exp. Med.* 188: 2019–2031.
16. Filgueira, L., F. O. Nestle, M. Rittig, H. I. Joller, and P. Groscurth. 1996. Human dendritic cells phagocytose and process *Borrelia burgdorferi*. *J. Immunol.* 157: 2998–3005.
17. Lyons, A. B., and C. R. Parish. 1994. Determination of lymphocyte division by flow cytometry. *J. Immunol. Methods* 171: 131–137.
18. Huang, F.-P., N. Platt, M. Wykes, J. R. Major, T. J. Powell, C. D. Jenkins, and G. G. MacPherson. 2000. A discrete subpopulation of dendritic cells transports apoptotic intestinal epithelial cells to T cell areas of mesenteric lymph nodes. *J. Exp. Med.* 191: 435–444.
19. Fulton, S. A., S. M. Reba, R. K. Pai, M. Pennini, M. Torres, C. V. Harding, and W. H. Boom. 2004. Inhibition of major histocompatibility complex II expression and antigen processing in murine alveolar macrophages by *Mycobacterium bovis* BCG and the 19-kilodalton mycobacterial lipoprotein. *Infect. Immun.* 72: 2101–2110.
20. Gonzalez-Juarrero, M., T. S. Shim, A. Kipnis, A. P. Junqueira-Kipnis, and I. M. Orme. 2003. Dynamics of macrophage cell populations during murine pulmonary tuberculosis. *J. Immunol.* 171: 3128–3135.
21. van Rijt, L. S., H. Kuipers, N. Vos, D. Hijdra, H. C. Hoogsteden, and B. N. Lambrecht. 2004. A rapid flow cytometric method for determining the cellular composition of bronchoalveolar lavage fluid cells in mouse models of asthma. *J. Immunol. Methods* 288: 111–121.
22. van der Merwe, P. A. 1999. A subtle role for CD2 in T cell antigen recognition. *J. Exp. Med.* 190: 1371–1374.
23. Williams, A. F., A. N. Barclay, S. J. Clark, D. J. Paterson, and A. C. Willis. 1987. Similarities in sequences and cellular expression between rat CD2 and CD4 antigens. *J. Exp. Med.* 165: 368–380.
24. Inaba, K., M. Witmer-Pack, M. Inaba, K. Hathcock, H. Sakuta, M. Azuma, H. Yagita, K. Okumura, P. Linsley, and S. Ikehara. 1994. The tissue distribution of the B7-2 costimulator in mice: abundant expression on dendritic cells in situ and during maturation in vitro. *J. Exp. Med.* 180: 1849–1860.
25. Holt, P. G., A. Degebrodt, C. O'Leary, K. Krska, and T. Plozza. 1985. T cell activation by antigen-presenting cells from lung tissue digests: suppression by endogenous macrophages. *Clin. Exp. Immunol.* 62: 586–593.
26. Bingisser, R. M., P. A. Tilbrook, P. G. Holt, and U. R. Kees. 1998. Macrophage-derived nitric oxide regulates T cell activation via reversible disruption of the Jak3/STAT5 signaling pathway. *J. Immunol.* 160: 5729–5734.
27. Kradin, R. L., K. M. McCarthy, W. Xia, D. Lazarus, and E. E. Schneeberger. 1991. Accessory cells of the lung. I. Interferon-gamma increases Ia^+ dendritic cells in the lung without augmenting their accessory activities. *Am. J. Respir. Cell Mol. Biol.* 4: 210–218.
28. Daffern, P. J., M. A. Jagels, J. J. Saad, W. Fischer, and T. E. Hugli. 1999. Upper airway epithelial cells support eosinophil survival in vitro through production of GM-CSF and prostaglandin E_2: regulation by glucocorticoids and TNF-α. *Allergy Asthma Proc.* 20: 243–253.
29. Brinker, K. G., H. Garner, and J. R. Wright. 2003. Surfactant protein A modulates the differentiation of murine bone marrow-derived dendritic cells. *Am. J. Physiol.* 284: L232–L241.
30. Brokaw, J. J., G. W. White, P. Baluk, G. P. Anderson, E. Y. Umemoto, and D. McDonald. 1998. Glucocorticoid-induced apoptosis of dendritic cells in the rat tracheal mucosa. *Am. J. Respir. Cell Mol. Biol.* 19: 598–605.
31. Holt, P. G., and J. A. Thomas. 1997. Steroids inhibit uptake and/or processing but not presentation of antigen by airway dendritic cells. *Immunology* 91: 145–150.
32. Suda, T., K. Chida, H. Matsuda, H. Hashizume, K. Ide, K. Yokomura, K. Suzuki, H. Kuwata, S. Miwa, H. Nakano, et al. 2003. High-dose intravenous glucocorticoid therapy abrogates circulating dendritic cells. *J. Allergy Clin. Immunol.* 112: 1237–1239.
33. McWilliam, A. S., A. M. Marsh, and P. G. Holt. 1997. Inflammatory infiltration of the upper airway epithelium during Sendai virus infection: involvement of epithelial dendritic cells. *J. Virol.* 71: 226–236.
34. Yagita, H., T. Nakamura, H. Karasuyama, and K. Okumura. 1989. Monoclonal antibodies specific for murine CD2 reveal its presence on B as well as T cells. *Proc. Natl. Acad. Sci. USA* 86: 645–649.
35. Inaba, K., W. J. Swiggard, M. Inaba, J. Meltzer, A. Mirza, T. Sasagawa, M. C. Nussenzweig, and R. M. Steinman. 1995. Tissue distribution of the DEC-205 protein that is detected by the monoclonal antibody NLDC-145. I. Expression on dendritic cells and other subsets of mouse leukocytes. *Cell. Immunol.* 163: 148–156.
36. Witmer-Pack, M. D., W. J. Swiggard, A. Mirza, K. Inaba, and R. M. Steinman. 1995. Tissue distribution of the DEC-205 protein that is detected by the monoclonal antibody NLDC-145. II. Expression in situ in lymphoid and nonlymphoid tissues. *Cell. Immunol.* 163: 157–162.
37. Steinman, R. M., D. Hawiger, and M. C. Nussenzweig. 2003. Tolerogenic dendritic cells. *Annu. Rev. Immunol.* 21: 685–711.
38. Sallusto, F., D. Lenig, R. Forster, M. Lipp, and A. Lanzavecchia. 1999. Two subsets of memory T lymphocytes with distinct homing potentials and effector functions. *Nature* 401: 708–712.
39. Langenkamp, A., M. Messi, A. Lanzavecchia, and F. Sallusto. 2000. Kinetics of dendritic cell activation: impact on priming of TH1, TH2 and nonpolarized T cells. *Nat. Immunol.* 1: 311–316.
40. Granucci, F., C. Vizzardelli, N. Pavelka, S. Feau, M. Persico, E. Virzi, M. Rescigno, G. Moro, and P. Ricciardi-Castagnoli. 2001. Inducible IL-2 production by dendritic cells revealed by global gene expression analysis. *Nat. Immunol.* 2: 882–888.
41. Angelini, G., S. Gardella, M. Ardy, M. R. Ciriolo, G. Filomeni, G. Di Trapani, F. Clarke, R. Sitia, and A. Rubartelli. 2002. Antigen-presenting dendritic cells provide the reducing extracellular microenvironment required for T lymphocyte activation. *Proc. Natl. Acad. Sci. USA* 99: 1491–1496.
42. de Heer, H. J., H. Hammad, T. Soullie, D. Hijdra, N. Vos, M. A. M. Willart, H. C. Hoogsteden, and B. N. Lambrecht. 2004. Essential role of lung plasmacytoid dendritic cells in preventing asthmatic reactions to harmless inhaled antigen. *J. Exp. Med.* 200: 89–98.
43. Wykes, M., A. Pombo, C. Jenkins, and G. G. MacPherson. 1998. Dendritic cells interact directly with naive B lymphocytes to transfer antigen and initiate class switching in a primary T-dependent response. *J. Immunol.* 161: 1313–1319.
44. Elliot, J. G., C. M. Jensen, S. Mutavdzic, J. P. Lamb, N. G. Carroll, and A. L. James. 2004. Aggregations of lymphoid cells in the airways of nonsmokers, smokers, and subjects with asthma. *Am. J. Respir. Crit. Care Med.* 169: 712–718.
45. Holt, P. G., S. Haining, D. J. Nelson, and J. D. Sedgwick. 1994. Origin and steady-state turnover of class II MHC-bearing dendritic cells in the epithelium of the conducting airways. *J. Immunol.* 153: 256–261.
46. Nelson, D. J., and P. G. Holt. 1995. Defective regional immunity in the respiratory tract of neonates is attributable to hyporesponsiveness of local dendritic cells to activation signals. *J. Immunol.* 155: 3517–3524.
47. Jahnsen, F. L., E. D. Moloney, T. Hogan, J. W. Upham, C. M. Burke, and P. G. Holt. 2001. Rapid dendritic cell recruitment to the bronchial mucosa of patients with atopic asthma in response to local allergen challenge. *Thorax* 56: 823–826.